

Article

Two-Dimensional Layered NiLiP₂S₆ Crystals as an Efficient Bifunctional Electrocatalyst for Overall Water Splitting

Song-Jeng Huang^{1,†}, Adil Muneeb^{1,2,†}, Palani Sabhapathy^{3,†}, Khasim Saheb Bayikadi², Tahir Murtaza², Kalaivanan Raju², Li-Chyong Chen^{3,4,*}, Kuei-Hsien Chen^{3,5,*} and Raman Sankar^{2,3,*}

- ¹ Department of Mechanical Engineering, National Taiwan University of Science and Technology, No. 43, Section 4, Keelung Road, Taipei 10607, Taiwan; sgjhuang@mail.ntust.edu.tw (S.-J.H.); adil.munir99@gmail.com (A.M.)
- ² Institute of Physics, Academia Sinica, Taipei 11529, Taiwan; khasimsaheb7@gmail.com (K.S.B.); tahirkas@gmail.com (T.M.); rskalaivanan@gmail.com (K.R.)
- ³ Center for Condensed Matter Sciences, National Taiwan University, Taipei 10617, Taiwan; sabhapathypalani@gmail.com
- ⁴ Center of Atomic Initiative for New Materials, National Taiwan University, Taipei 10617, Taiwan
- ⁵ Institute of Atomic and Molecular Sciences, Academia Sinica, Taipei 10617, Taiwan
- * Correspondence: chenlc@ntu.edu.tw (L.-C.C.); chenkh@pub.iam.s.sinica.edu.tw (K.-H.C.); sankarraman@gate.sinica.edu.tw (R.S.)
- † Equal contribution.



Citation: Huang, S.-J.; Muneeb, A.; Sabhapathy, P.; Bayikadi, K.S.; Murtaza, T.; Raju, K.; Chen, L.-C.; Chen, K.-H.; Sankar, R. Two-Dimensional Layered NiLiP₂S₆ Crystals as an Efficient Bifunctional Electrocatalyst for Overall Water Splitting. *Catalysts* **2021**, *11*, 786. <https://doi.org/10.3390/catal11070786>

Academic Editors: Sabrina Campagna Zignani and José Joaquín Linares León

Received: 4 June 2021
Accepted: 25 June 2021
Published: 28 June 2021

Publisher's Note: MDPI stays neutral with regard to jurisdictional claims in published maps and institutional affiliations.



Copyright: © 2021 by the authors. Licensee MDPI, Basel, Switzerland. This article is an open access article distributed under the terms and conditions of the Creative Commons Attribution (CC BY) license (<https://creativecommons.org/licenses/by/4.0/>).

Abstract: The quest of earth-abundant bifunctional electrocatalysts for highly efficient oxygen evolution reaction (OER) and hydrogen evolution reaction (HER) is essential for clean and renewable energy systems. Herein, directed by the experimental analysis, we demonstrate layered nickel lithium phosphosulfide (NiLiP₂S₆) crystal as a highly efficient water-splitting catalyst in alkaline media. With strained lattice due to stacked layers as observed by TEM and electronic structure analysis performed by XPS showed mixed Ni^{2+,3+} oxidation states induced by addition of Li as a cation, NiLiP₂S₆ displays excellent OER (current density of 10 mA cm⁻² showed an overpotential of 303 mV vs. RHE and a Tafel slope of 114 mV dec⁻¹) and HER activity (current density of -10 mA cm⁻² showed an overpotential of 184 mV vs. RHE and a Tafel slope of 94.5 mV dec⁻¹). Finally, an alkaline media was employed to demonstrate the overall water splitting using NiLiP₂S₆ as both the anode and the cathode, which attained a 50 mA cm⁻² current density at 1.68 V. This bimetallic phosphosulfide, together with long-term stability and enhanced intrinsic activity, shows enormous potential in water splitting applications.

Keywords: water splitting; bifunctional electrocatalyst; HER (hydrogen evolution reaction); OER (oxygen evolution reaction)

1. Introduction

The overuse of fossil fuels has led to rapid climate change, global warming, and a shortage of natural reserves, and pushed us to quest for sustainable and alternative energy sources [1]. Hydrogen energy (H₂) produced by water electrolysis is purer, environmentally benign and generates low carbon emissions, and has long been pursued as an alternative to fossil fuels [2,3]. Active oxygen and hydrogen evolution reaction (OER and HER) electrocatalysts are desired to enhance the reaction rate at low-overpotential for catalyzation of bond-forming and bond-breaking reactions [4]. Platinum-based group metals and their oxides (e.g., IrO₂ and RuO₂) have been employed as the most efficient commercial OER and HER catalysts owing to their surface transient states for oxygen electrode reactions [5]. However, IrO₂-Pt needs a larger cell voltage (1.75–2.0 V) than the thermodynamic value (1.23 V) to maintain commercially viable current density as a water electrolyzer [6]. Unfortunately, factors like catalyst deterioration over long-term performance, scarcity, and high costs have limited their scope for large-scale industrialization [7].

Accordingly, it is crucial to seek highly effective, durable, and earth-abundant catalysts to realize the commercialization of water electrolyzers with less energy consumption at large scales [8]. Owing to their thermodynamic advantages, a series of materials such as layered metal hydroxides [9] and metal perovskite oxides [10,11] were investigated as efficient OER catalysts, and materials like phosphides [12], phosphosulfides [13], sulfides [14], disulfides [15], transition metal dichalcogenides [16], selenides [17], and carbon-based catalysts [18] were studied as potential HER catalysts.

Layered metal transition thiophosphates were first discovered in late 1894 [19] and, later, described in more detail by Ferrand [20]. Structurally all members in this class of materials share common $P_2(\text{Se/S})_6$ sublattice anion within every layer. The cation side can accommodate alkali and alkaline earth elements, transition metals, and some heavier elements like Ag, Cd, and Pb with $[P_2\text{Se}_6]^{4-}$ and $[P_2\text{S}_6]^{4-}$ anions. Considering their structural variations, which give rise to interesting magnetic and electronic properties, one can see classifications immediately span a vast breadth of materials extensive research work, ranging from magnetic properties [21] to applications like H_2 storage [22] and Li-ion batteries [23].

Based on the reported citation, $\text{Mn}_2\text{P}_2\text{S}_6$ shows superior performance in oxygen reduction reaction (ORR), and $\text{Co}_2\text{P}_2\text{S}_6$ exhibits excellent OER performance [24]. In particular, $\text{Fe}_2\text{P}_2\text{S}_6$ and $\text{Ni}_2\text{P}_2\text{S}_6$ are the attractive members and most studied materials for this family of materials, considering their magnetic ordering and large Li^+ ions storage capacity. Barj et al. [25] reported the lithium intercalation Li_xMPS_3 with $\text{M} = \text{Ni}, \text{Fe}$ in the range of $0 < x < 1.5$ and concluded that Li^+ ions settle 2d and 4h octahedral sites which give rise to best energy yields for superior electrochemical performance. However, if the intercalated species is charged, overall electroneutrality is maintained by metal cations either (a) being reduced (as in the case of lithium intercalation in $\text{Ni}_2\text{P}_2\text{S}_6$ and $\text{Fe}_2\text{P}_2\text{S}_6$) or (b) leaving the structure to maintain the charge balance. This can affect the overall electrochemical performance.

To the best of our knowledge, until this date, no reports have been published on the inclusion of Li as a cation in the layered nickel phosphosulfide. Here we report novel NiLiP_2S_6 as a layered material using the chemical vapor transport method (CVT). Information about crystal structure and space group are described in detail. As prepared few-layered NiLiP_2S_6 crystals were washed and used directly as bifunctional OER/HER catalyst in alkaline media. A three-electrode cell configuration employing 1 M KOH electrolyte, NiLiP_2S_6 crystals showed excellent electrochemical performance as a bifunctional catalyst for OER and HER. Together with long-term stability and durability, it indicates enormous potential as a water electrolyzer catalyst.

2. Results and Discussion

X-ray diffraction (XRD) pattern of NLPS and Rietveld refinement analysis results are shown in Figure 1a. Rietveld analysis further revealed that the NLPS sample belongs to the monoclinic crystal structure (space group $A2/m$, $a = 5.99$ (2) Å, $b = 11.06$ (10) Å, $c = 13.54$ (9) Å, $\beta = 105.99^\circ$ (3)), confirming the single-phase product. A close examination of the sharp diffraction peak around 13.8° indicates high crystallinity in the layered structure sample. The crystallite size and strain values at the major peak calculated from the XRD data were 37.65 nm and 7.3×10^{-3} respectively. Table S1 contains the crystallite size and strain values for other major peak intensities. Table S2 enlists the reliability factors of Rietveld refinement analysis, information about atomic coordinates, and unit cell volume. Figure 1b shows NLPS crystal structure exhibiting layers of phosphorous and alkali metal atoms sandwiched between the sulfur layers, forming a honeycomb pattern. This facilitates the alkali metal atoms intercalation in the layered structure. This kind of ordered intercalated layered structure would give rise to spin imbalance as proposed in the model by Evans et al. [26] which possibly explains the superior bifunctional catalytic activity for HER and OER. Figure 1c shows crystal structure in a 2×2 layer arrangement displaying alternating honeycomb structure. Figure S2 shows the inter atomic distances between

individual atoms. The structure and morphology of layered NLPS single crystal are further characterized by Transmission and Scanning Electron Microscopy (TEM and SEM).

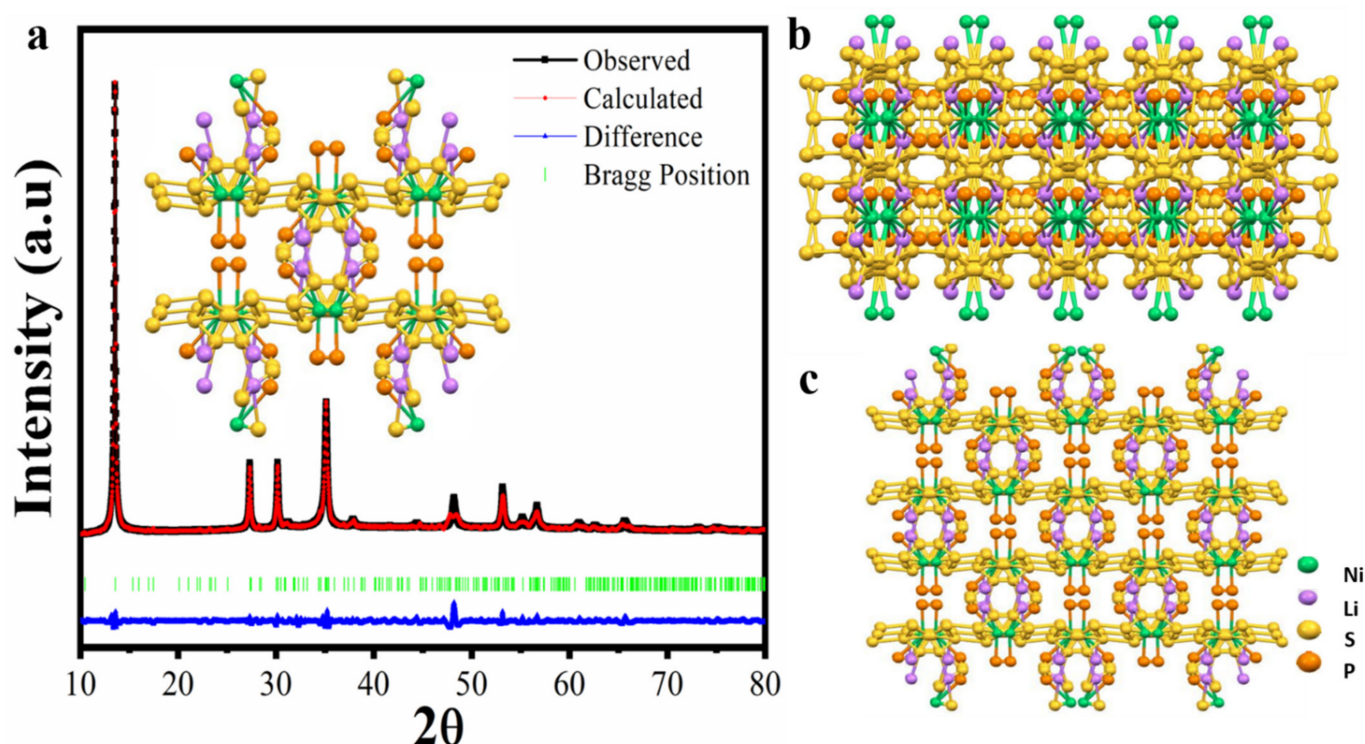


Figure 1. Experimental and simulated Rietveld refinement analysis and crystal structure of NLPS: (a) Rietveld analysis of X-ray powder diffraction data of NiLiP_2S_6 and unit cell; (b) complete crystal structure; (c) asymmetrical 2×2 layer crystal structure.

SEM analysis shows layer by layer stacking of a single crystal, as seen in Figure 2a. A single crystal was cleaved and TEM analysis was performed. Figure 2b displays a cleaved thin layer of single crystal, with the presence of strain along the boundaries of the individual lamella stacked on top of each other. Figure 2c represents stacked layers of a single crystal. Moreover, the HRTEM image confirms the high crystallinity and clearly showing hexagonal lattice. Figure 2d illustrates the high-resolution image as well as strain analysis of NLPS single crystal. The origin of strain can be explained by the presence of layer by layer stacking in NLPS. Liu et al. [27] explored a metal thiophosphate band structure in water-splitting reaction computationally. It was observed that the presence of strain counter-intuitively somehow decreases the bandgap, thus, making these materials excellent in water splitting due to tunable band structure. This in turn, presents the most effective combination of electronegativity and electron affinity allows redox of $\text{O}_2/\text{H}_2\text{O}$ and $\text{H}^+/\text{H}_2\text{O}$ to be placed below the valence band maximum and conduction band minimum, respectively. The red inset in Figure 2d clearly shows a hexagonal lattice while the top right inset shows a hexagonal pattern along the (010) plane and the observation matches well with X-ray analysis. D-spacing analysis was performed and demonstrated in Figure 2e. The calculated value along the (131) plane is found to be 2.93 \AA , which is matched with powder X-ray Rietveld refinement analysis. Selective area electron diffraction pattern (SAED) in Figure 2f reveals some hexagonal superlattice. The origin of the superlattice can be due to the metal ions intercalation. Another reason could be due to strain, which in principle is responsible for atomic bonding directly and presents an ideal platform for tuning surface catalysis [28]. This explains the enhanced bi-functional catalytic performance of NLPS.

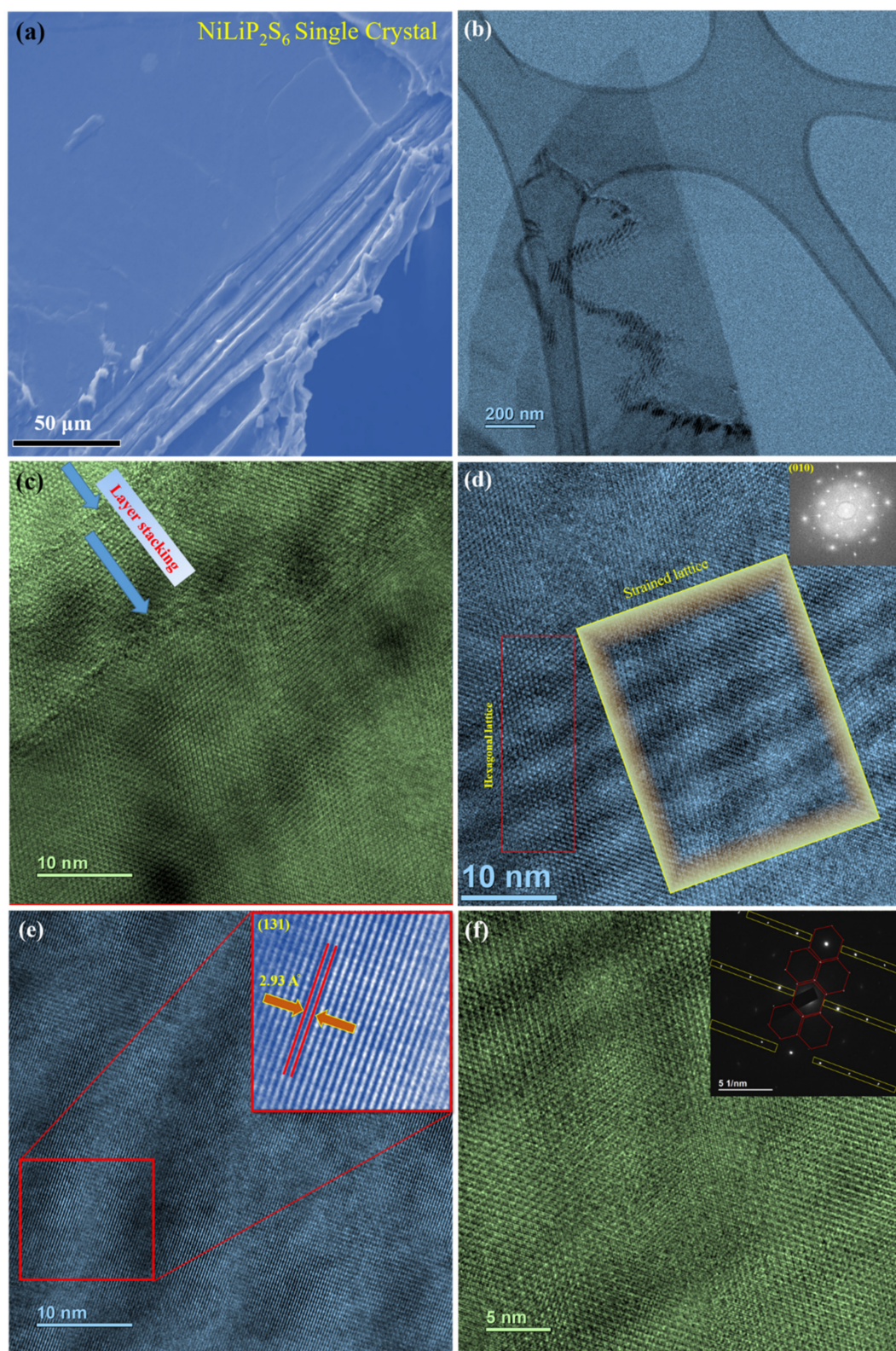


Figure 2. Scanning and Transmission Electron Microscopy images of NLPS: (a) SEM image of layered Single crystal. (b) HRTEM image of cleaved thin layer single crystal. (c) HRTEM image exhibiting layered stacking of single crystal. (d) HRTEM image displaying strain lattice with top-right inset shows a hexagonal pattern. (e) Inset at the upper right corner shows d-spacing between atoms along with atoms arrangement. (f) Inset at the upper right corner shows SAED (selective area electron diffraction pattern) and super lattice.

Furthermore, composition and valence state, as well as the bonding characteristics of NLPS, were further analyzed by XPS. The analysis confirms the presence of lithium, nickel, phosphorous, and sulfur species, as shown in Figure 3. Figure 3a shows Ni core-level spectra and distribution of Ni²⁺ and Ni³⁺. The Ni/Li cation peak ratio intensities obtained from the XPS analyses of the NLPS sample were very close to the original stoichiometry values during the initial analysis. The core-level spectrum of Ni 2p has its spin-orbit doublet into high energy Ni 2p_{3/2} and low energy Ni 2p_{1/2} regions, respectively. Oxidation states of Ni 2p_{3/2} prominent peaks were found at a B.E of 854.7 eV with the relative intensity of Ni²⁺ > Ni³⁺. Moreover, the satellite feature was positioned at 859.8 eV. The binding state of low energy Ni 2p_{1/2} peak was located at the binding energy of 872.3 eV with a little difference in intensities of Ni²⁺ and Ni³⁺ ions. The satellite feature was positioned at 877.3 eV. The core-level spectrum of P 2p (Figure 3b) and S 2p (Figure 3c) region show spin doublets 2p_{1/2} and 2p_{3/2} without any traces of oxides and additional phases. The oxidation state of P⁴⁺ and S²⁻ were located at the B.E of 132 eV (P 2p_{3/2}) and 165 eV (S 2p_{3/2}), respectively. Figure 3d shows Li 1s core-level spectra. The asymmetric peak positioned around 55.3 ± 0.06 eV rules out decisively the presence of any contaminated species and confirmed the presence of pure Li⁺ metal ion. Moreover, it is impossible to avoid surface oxidation of layered materials under longtime exposition into the air atmosphere. As shown in Figure S3, the surface of the NLPS get oxidized after longtime expose to air.

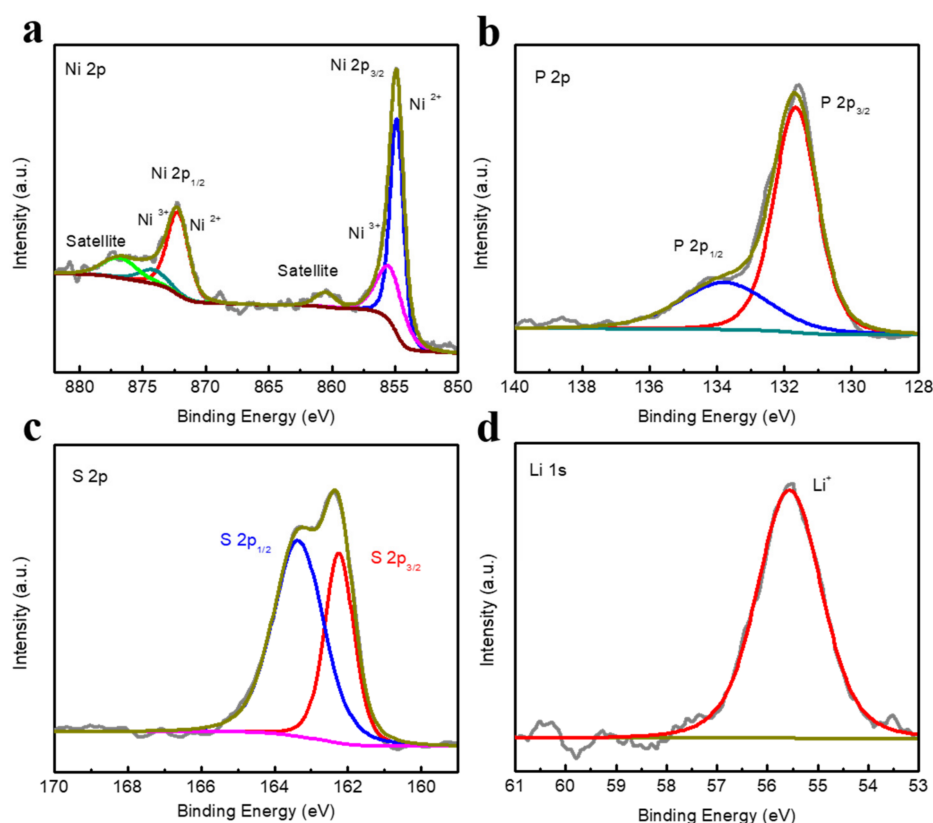


Figure 3. XPS (X-ray photoelectron spectroscopy) of the NLPS, (a) Ni 2p spectra, (b) P 2p spectra, (c) S 2p spectra, (d) Li 1s spectra.

A standard three-electrode system was used to investigate the OER activity of NLPS on nickel foam (called NLPS/Ni foam) in 1 M KOH solution. The linear sweep voltammetry (LSV) curves of NLPS/Ni foam and bare nickel foam are shown. As displayed in Figure 4a, NLPS/Ni foam shows the most prominent catalytic current activity for OER at 10 mA cm⁻² with the smallest overpotential of 303 mV at the expense of lowest onset potential of ~1.48 V vs. RHE. When the anodic current density reached 50 mA cm⁻², the respective

over potentials of the NLPS/Ni foam and Ni foam were 330 and 470 mV. This indicates the superior OER activity of NLPS/Ni foam.

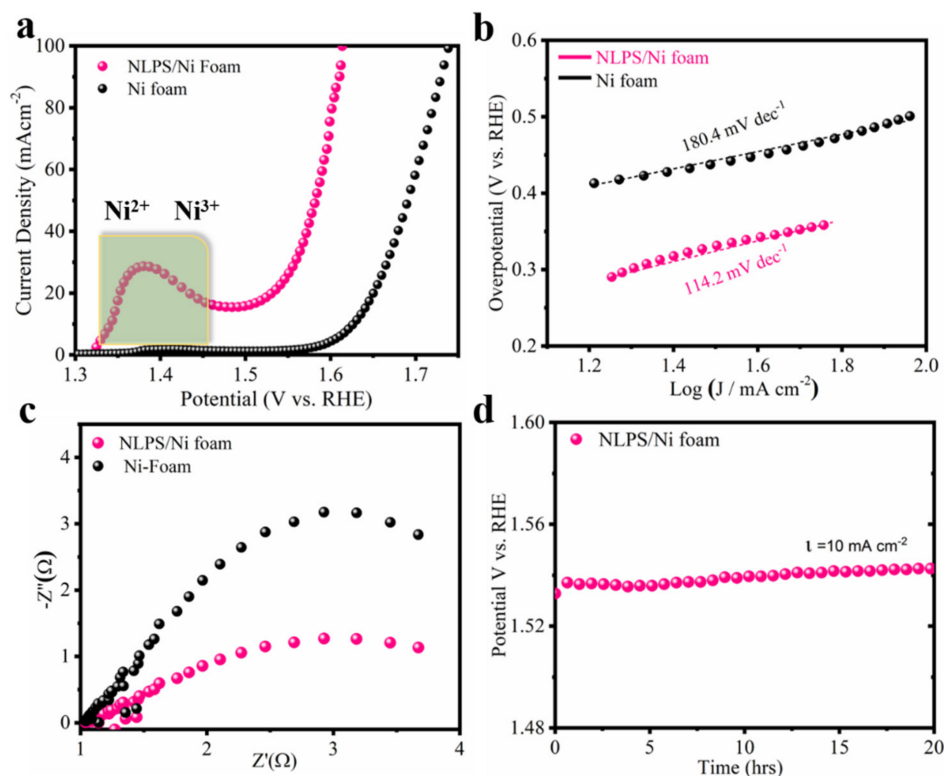


Figure 4. OER electrocatalytic performance in alkaline media. (a) Polarization LSV curves and (b) Tafel plots of NLPS/Ni foam and Ni foam; (c) EIS Nyquist Plot for catalysts; (d) durability test of NLPS/Ni foam at 10 mA cm^{-2} .

Furthermore, Tafel plots (derived from polarization LSV curves) were used to evaluate the OER process kinetics as shown in Figure 4a. As can be seen from Figure 4b, the NLPS/Ni foam displays the minimal Tafel slope value of $114.2 \text{ mV dec}^{-1}$, which is superior than Ni foam ($180.4 \text{ mV dec}^{-1}$). This explains the fastest OER process kinetics of NLPS/Ni foam catalyst. EIS (Electrochemical impedance spectroscopy) was performed to investigate kinetics. While comparing the NLPS/Ni foam and Ni foam, it was observed that NLPS/Ni foam displays a remarkably lower charge-transfer resistance (Figure 4c). The electrochemical impedance spectroscopy data confirms that the NLPS/Ni foam shows rapid charge-transfer during the catalytic reaction, which matches well with the results of low Tafel slope and more positive onset potential. In addition, to evaluate the overall catalytic performance in practice, the high OER durability of catalyst is very crucial. For that reason, the OER durability of the NLPS/Ni foam was recorded. The time-dependent NLPS/Ni foam current density profile was evaluated for 20 h under a constant current density of 10 mA cm^{-2} . Figure 4d indicates that NLPS/Ni foam exhibits excellent stability toward OER.

A standard three-electrode system was employed to evaluate the HER activity of NLPS on nickel foam (called NLPS/Ni foam), Ni foam, and standard Pt/C in alkaline media. The LSV polarization curves displays that NLPS/Ni foam undergoes a relatively small value of 184 mV overpotential to attain a current density of 10 mA cm^{-2} , notably lower than the 276 mV of Ni foam (Figure 5a). As expected, Pt/C displays smallest onset potential (around-zero) and undergoes 50 mV of overpotential value at 10 mA cm^{-2} current density. Figure 5b shows the NLPS/Ni foam Tafel slope value of 94.5 mV dec^{-1} , which is considerably lower than pure Ni foam ($145.3 \text{ mV dec}^{-1}$). This shows that the NLPS/Ni foam has effective HER electron transfer. As shown in Figure 5c, the chronopotentiometry

test for NLPS/Ni foam at $j = 20 \text{ mA cm}^{-2}$ shows that the overpotential is nearly constant during the continuous operation for 20 h. Besides, effective electrode surface area was evaluated by measuring Cdl (electrochemical double-layer capacitance). NLPS/Ni foam exhibits the largest Cdl of 3.6 mF cm^{-2} , which is much larger than Ni foam (0.8 mF cm^{-2}), demonstrating the most considerable exposure of effective active sites (Figure 5d and Figure S4). Further, a whole-cell water electrolyzer was employed in 1 M KOH, while for both anode and cathode, NLPS/Ni foam was used. The polarization LSV curve of the NLPS/Ni foam cell was measured and compared to the cell constructed using Ni foam. As shown in Figure 6a, the NLPS/Ni foam cell displays better performance to the Ni foam cell. The potential required for a whole-cell water electrolyzer in the case of NLPS/Ni foam is only 1.68 V (without iR -correction) to attain current density of 50 mA cm^{-2} , which is better than Ni foam (1.8 V at 20 mA cm^{-2}). The NLPS/Ni foam cell also exhibits excellent long-term stability during the 20 h bulk water electrolysis at $j = 50 \text{ mA cm}^{-2}$ (Figure 6b). In order to prove the intrinsic activity of NLPS catalyst, the current density of overall water splitting reaction was normalized by ECSA. As shown in Figure S4c, after being normalized by ECSA, the current density still shows better than pure Ni foam. Figure 6c shows the schematic illustration of the NLPS/Ni foam electrode for overall water splitting as both the anode and the cathode.

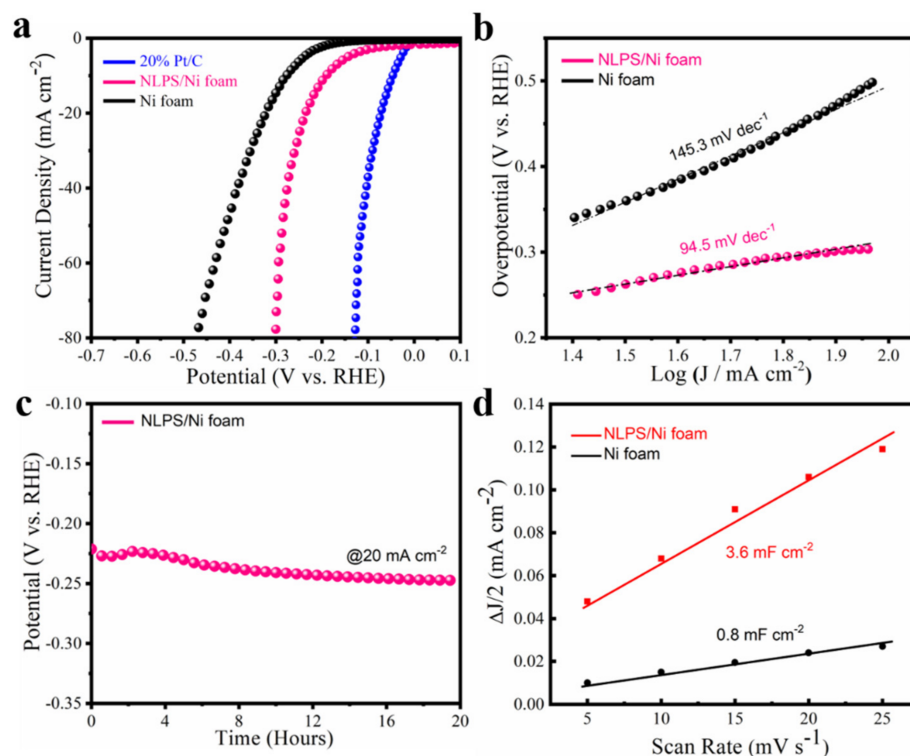


Figure 5. HER electrocatalytic performance in alkaline media. (a) Polarization LSV curves and (b) Tafel plots of NLPS/Ni foam and Ni foam; (c) durability test of NLPS/Ni foam at -20 mA cm^{-2} ; (d) linear plot of Δj vs. scan rate of NLPS/Ni foam.

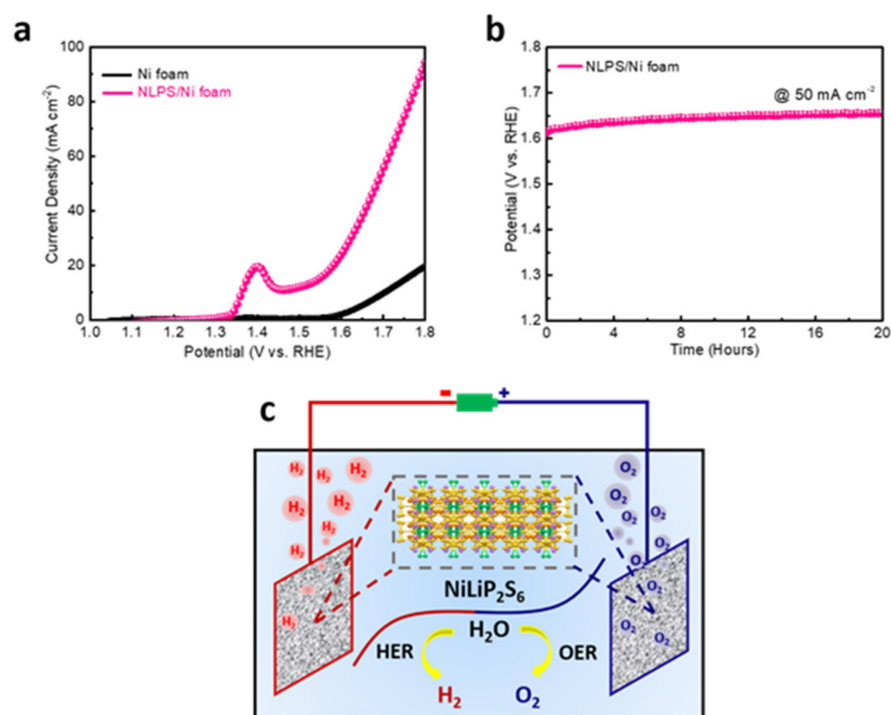


Figure 6. Overall water splitting in alkaline media. (a) Polarization LSV curves of NLPS/Ni foam and Ni foam; (b) durability test of NLPS/Ni foam at 50 mA cm⁻²; (c) schematic illustration of NLPS/Ni foam electrode as both the anode and cathode for overall water splitting.

3. Materials and Methods

3.1. Preparation of NiLiP₂S₆ (NLPS) Crystal

NiLiP₂S₆ crystals were synthesized via the chemical vapor transport (CVT) method. Lithium sulfide (Li₂S) powder (Alfa Aesar, 99.99%, Ward Hill, MA, USA), Sulphur powder (Alfa Aesar, 99.99%, Ward Hill, MA, USA), nickel powder (Alfa Aesar, 99.99%, Ward Hill, MA, USA), and phosphorous red lump (Alfa Aesar, 99.999%, Alfa Aesar, 99.99%, Ward Hill, MA, USA) were used as a starting precursor for compound growth. A stoichiometric amount of precursors was mixed in the Ar atmosphere glovebox and subsequently sealed in a quartz tube with 10⁻⁴ to 10⁻⁵ torr of an internal pressure. Initially, the compound was heated for 10 h, followed by the grinding. Compound was sealed again in a quartz tube under similar conditions and put for a second round of heating at 600 °C for 24 h. Finally, the compound was ground again inside the glove box and sealed quartz tubes were subjected to a dual-zone horizontal tube furnace (700 °C–600 °C for 200 h) for one week. Fine quality crystals were collected and washed with ethanol as shown in Figure S1.

3.2. Structural Characterization

X-ray Powder Diffraction was obtained by using powder D2 phaser Bruker X-ray diffractometer with wavelength $\lambda = 1.54 \text{ \AA}$ (Cu-K α radiation) operated at 30 mA and 40 kV (Bruker, Ettlingen., Germany). Structural morphology was characterized by employing SEM (scanning electron microscopy) 8020SU, Hitachi at 2 KV voltage equipped with the EDX (energy-dispersive X-ray spectroscopy, Hitachi, Mannheim., Germany). HRTEM (high-resolution transmission electron microscopy) pictures were recorded using the STWIN F30 G2 Tecnai instrument having a 200 KV capacity for gun (FEI, Yumpu., Switzerland). X-ray spectroscopy (XPS) analysis was performed on a VG ESCA Scientific theta probe using AlK α monochromatic as the exciting source (Thermo fisher scientific, Waltham, MA, USA). Au 4f peaks were used to carefully calibrate the peak intensity positions of XPS. For background subtraction, Shirley procedure was used and later Voigt fitting function was employed for deconvolution of individual XPS spectra's. ETMs were placed on

PEDOT/ITO: a 20-s time interval was used for 1 KeV ion-energy to hit the interface of specimen. Carbon peak recorded at 284.5 eV was used as reference for all B.E. In order to fit the XPS data, GL (Gaussian Lorentzian) function and Shirley background was taken in to account.

3.3. Electrochemical Measurements

Commercial Ni foam (NF) with 1.6 mm thickness and 350 g/m³ density was cut into small pieces approximately 2 cm² (working area 1 × 1 cm²) in the area and subsequently sonicated with 1 M HCL, ethanol, and DI water for 30 min each. A total of 10 mg of catalyst dissolved in 1035 µL of 35 µL of Nafion and isopropanol/water solvent 1:1. A homogenous ink was obtained by stirring the mixture followed by 50 min sonication. A total of 100 µL of ink solution drop cast on NF (1 × 1 cm²) was used as working electrode (approximately 0.94 mg cm⁻²), Ag/AgCl electrode (saturated KCl solution, 0.197 V vs. RHE), and graphite rod were used as counter and reference electrodes, respectively. All the electrochemical performance was measured in alkaline media (1M KOH). Oxygen and hydrogen evolution reaction (OER) and (HER) polarization LSV curves were achieved in N₂ saturated electrolyte by LSV at a scan rate of 5 mV s⁻¹ (30% iR compensation value was used). Electrochemical impedance spectroscopy (EIS) was recorded in the frequency range from 0.1 Hz to 100 kHz.

3.4. Overall Water Splitting Test

In order to conduct the overall water electrolysis test, a three-electrode configuration having Ag/AgCl as a reference electrode was used. The anode and cathode was carefully prepared by drop-casting the prepared NLPS/Ni foam catalyst ink onto Ni foam with a controlled catalyst loading density of 1mg cm⁻². The overall water splitting measurements were carried out in a de-aerated 1M KOH aqueous solution. The geometric area of the catalyst was used to normalize the current density (measurements performed without iR compensation).

4. Conclusions

To summarize, novel layered NiLiP₂S₆ crystals were obtained from chemical vapor transport method, and their bifunctional electrochemical properties were investigated. Further, crystal structure was discussed in detail along with the impact of strain in the layered lamella on electrochemical properties. NLPS/Ni foam display excellent HER electrochemical activity with a minimal overpotential of 184 mV vs. RHE for j = -10 mA cm⁻² current density and a Tafel slope of 94 mV dec⁻¹. Similarly, NLPS/Ni foam shows excellent OER activity with a minimal overpotential of 303 mV vs. RHE for j = 10 mA cm⁻² current density and a Tafel slope of 114.2 mV dec⁻¹, making it an excellent bifunctional catalyst better than many reported materials. Concertedly with promising long term durability for 20 h, it is expected that such layered metal phosphosulfide catalyst have great potential for renewable energy storage systems.

Supplementary Materials: The following are available online at <https://www.mdpi.com/article/10.3390/catal11070786/s1>, Figure S1: As Synthesized NLPS crystals, Figure S2: XRD Pattern of NiLiP₂S₆, Figure S3: O 1s XPS spectra, Figure S4: Cyclic voltammetry at different scan rates (a) NLPS. (b) Ni foam, Table S1: Structural parameters of the catalysts obtained from Rietveld refinement of XRD powder data. Table S2: Structural parameters of the catalysts obtained from Ritveld refinement of XRD powder data.

Author Contributions: Conceptualization, methodology, investigation and writing S.-J.H., A.M. and P.S.; methodology and investigation, K.S.B., T.M., K.R.; supervision, L.-C.C., K.-H.C. and R.S. All authors have read and agreed to the published version of the manuscript.

Funding: R.S. acknowledges financial support provided by the Ministry of Science and Technology (MOST) in Taiwan under project number MOST-108-2112-M-001-049-MY2 as well as Academia Sinica for the budget of AS-iMate-109-13. L.C.C. and K.H.C. acknowledges financial support provided by

the Ministry of Science and Technology (MOST) in Taiwan, under the Academic Summit Project 107-2745-M-002-001-ASP and the Science Vanguard Project (108-2119-M-002-030 and 109-2123-M-002-004). Financial supports were also provided by the i-MATE program in Academia Sinica (AS-iMATE-108-31).

Conflicts of Interest: The authors declare no conflict of interest.

References

1. De Luna, P.; Hahn, C.; Higgins, D.; Jaffer, S.A.; Jaramillo, T.F.; Sargent, E.H. What would it take for renewably powered electrosynthesis to displace petrochemical processes? *Science* **2019**, *364*, eaav3506. [[CrossRef](#)] [[PubMed](#)]
2. Tang, C.; Gan, L.; Zhang, R.; Lu, W.; Jiang, X.; Asiri, A.M.; Sun, X.; Wang, J.; Chen, L. Ternary Fe x Co 1–x P Nanowire Array as a Robust Hydrogen Evolution Reaction Electrocatalyst with Pt-like Activity: Experimental and Theoretical Insight. *Nano Lett.* **2016**, *16*, 6617–6621. [[CrossRef](#)]
3. Zhang, X.; Zhang, S.; Li, J.; Wang, E. One-step synthesis of well-structured NiS–Ni 2 P 2 S 6 nanosheets on nickel foam for efficient overall water splitting. *J. Mater. Chem. A* **2017**, *5*, 22131–22136. [[CrossRef](#)]
4. Shi, H.; Liang, H.; Ming, F.; Wang, Z. Efficient Overall Water-Splitting Electrocatalysis Using Lepidocrocite VOOH Hollow Nanospheres. *Angew. Chemie Int. Ed.* **2017**, *56*, 573–577. [[CrossRef](#)]
5. Solmaz, R.; Gündoğdu, A.; Döner, A.; Kardaş, G. The Ni-deposited carbon felt as substrate for preparation of Pt-modified electrocatalysts: Application for alkaline water electrolysis. *Int. J. Hydrog. Energy* **2012**, *37*, 8917–8922. [[CrossRef](#)]
6. Morales-Guio, C.G.; Stern, L.-A.; Hu, X. Nanostructured hydrotreating catalysts for electrochemical hydrogen evolution. *Chem. Soc. Rev.* **2014**, *43*, 6555. [[CrossRef](#)] [[PubMed](#)]
7. Luo, F.; Zhang, Q.; Yu, X.; Xiao, S.; Ling, Y.; Hu, H.; Guo, L.; Yang, Z.; Huang, L.; Cai, W.; et al. Palladium Phosphide as a Stable and Efficient Electrocatalyst for Overall Water Splitting. *Angew. Chemie Int. Ed.* **2018**, *57*, 14862–14867. [[CrossRef](#)]
8. Wang, J.; Zhong, H.; Wang, Z.; Meng, F.; Zhang, X. Integrated Three-Dimensional Carbon Paper/Carbon Tubes/Cobalt-Sulfide Sheets as an Efficient Electrode for Overall Water Splitting. *ACS Nano* **2016**, *10*, 2342–2348. [[CrossRef](#)] [[PubMed](#)]
9. Zhang, B.; Zheng, X.; Voznyy, O.; Comin, R.; Bajdich, M.; Garcia-Melchor, M.; Han, L.; Xu, J.; Liu, M.; Zheng, L.; et al. Homogeneously dispersed multimetal oxygen-evolving catalysts. *Science* **2016**, *352*, 333–337. [[CrossRef](#)]
10. Hirai, S.; Ohno, T.; Uemura, R.; Maruyama, T.; Furunaka, M.; Fukunaga, R.; Chen, W.-T.; Suzuki, H.; Matsuda, T.; Yagi, S. Ca 1–x Sr x RuO 3 perovskite at the metal–insulator boundary as a highly active oxygen evolution catalyst. *J. Mater. Chem. A* **2019**, *7*, 15387–15394. [[CrossRef](#)]
11. Huang, S.-J.; Muneeb, A.; Sabhapathy, P.; Sheelam, A.; Bayikadi, K.S.; Sankar, R. Tailoring the Co 4+ /Co 3+ active sites in a single perovskite as a bifunctional catalyst for the oxygen electrode reactions. *Dalt. Trans.* **2021**. [[CrossRef](#)]
12. Lado, J.L.; Wang, X.; Paz, E.; Carbó-Argibay, E.; Guldris, N.; Rodríguez-Abreu, C.; Liu, L.; Kovnir, K.; Kolen'ko, Y.V. Design and Synthesis of Highly Active Al–Ni–P Foam Electrode for Hydrogen Evolution Reaction. *ACS Catal.* **2015**, *5*, 6503–6508. [[CrossRef](#)]
13. Kibsgaard, J.; Jaramillo, T.F. Molybdenum Phosphosulfide: An Active, Acid-Stable, Earth-Abundant Catalyst for the Hydrogen Evolution Reaction. *Angew. Chemie Int. Ed.* **2014**, *53*, 14433–14437. [[CrossRef](#)]
14. Yang, Y.J.; Hu, X. Nanoporous Ni 3 S 2 Film on Ni Foam as Highly Efficient Electrocatalyst for Hydrogen Evolution in Acidic Electrolyte. *Russ. J. Electrochem.* **2019**, *55*, 88–96. [[CrossRef](#)]
15. Escalera-López, D.; Niu, Y.; Yin, J.; Cooke, K.; Rees, N.V.; Palmer, R.E. Enhancement of the Hydrogen Evolution Reaction from Ni–MoS 2 Hybrid Nanoclusters. *ACS Catal.* **2016**, *6*, 6008–6017. [[CrossRef](#)] [[PubMed](#)]
16. Lv, R.; Robinson, J.A.; Schaak, R.E.; Sun, D.; Sun, Y.; Mallouk, T.E.; Terrones, M. Transition Metal Dichalcogenides and Beyond: Synthesis, Properties, and Applications of Single- and Few-Layer Nanosheets. *Acc. Chem. Res.* **2015**, *48*, 56–64. [[CrossRef](#)]
17. Kong, D.; Wang, H.; Lu, Z.; Cui, Y. CoSe 2 Nanoparticles Grown on Carbon Fiber Paper: An Efficient and Stable Electrocatalyst for Hydrogen Evolution Reaction. *J. Am. Chem. Soc.* **2014**, *136*, 4897–4900. [[CrossRef](#)] [[PubMed](#)]
18. Duan, J.; Chen, S.; Jaroniec, M.; Qiao, S.Z. Porous C 3 N 4 Nanolayers@N-Graphene Films as Catalyst Electrodes for Highly Efficient Hydrogen Evolution. *ACS Nano* **2015**, *9*, 931–940. [[CrossRef](#)] [[PubMed](#)]
19. Académie des Sciences (Paris). National de la recherche scientifique. In *Comptes Rendus Hebdomadaires des Séances de l'Académie des Sciences*; publiés avec le concours du Centre national de la recherche scientifique par MM; Les Secrétaires Perpétuels: Paris, France, 1835; Volume 1, ISBN 0001-4036.
20. Brec, R. Review on structural and chemical properties of transition metal phosphorous trisulfides MPS3. *Solid State Ionics* **1986**, *22*, 3–30. [[CrossRef](#)]
21. Dziaugys, A.; Banyas, J.; Macutkevicius, J.; Sobiestianskas, R.; Vysochanskii, Y. Dipolar glass phase in ferrielectrics: CuInP 2 S 6 and Ag 0.1 Cu 0.9 InP 2 S 6 crystals. *Phys. Status Solidi* **2010**, *207*, 1960–1967. [[CrossRef](#)]
22. Ismail, N.; El-Meligi, A.A.; Temerk, Y.M.; Madian, M. Synthesis and characterization of layered FePS3 for hydrogen uptake. *Int. J. Hydrog. Energy* **2010**, *35*, 7827–7834. [[CrossRef](#)]
23. GARD, P.; SOURISSEAU, C.; OUVREARD, G.; BREC, R. Infrared study of lithium intercalated phases in the Li_xFeS₂ system (0 ≤ x ≤ 2). Characterization of a new iron disulfide. *Solid State Ionics* **1986**, *20*, 231–238. [[CrossRef](#)]
24. Mayorga-Martinez, C.C.; Sofer, Z.; Sedmidubský, D.; Huber, Š.; Eng, A.Y.S.; Pumera, M. Layered Metal Thiophosphite Materials: Magnetic, Electrochemical, and Electronic Properties. *ACS Appl. Mater. Interfaces* **2017**, *9*, 12563–12573. [[CrossRef](#)] [[PubMed](#)]

25. Barj, M. Infrared studies of lithium intercalation in the FePS₃ and NiPS₃ layer-type compounds. *Solid State Ionics* **1983**, *11*, 179–183. [[CrossRef](#)]
26. Evans, J.S.O.; O'Hare, D.; Clement, R. The Structure of Co(eta-C₅H₅)₂⁺ and NMe₄⁺ Intercalates of MnPS₃: An X-ray, Neutron-Diffraction, and Solid-State NMR Study. *J. Am. Chem. Soc.* **1995**, *117*, 4595–4606. [[CrossRef](#)]
27. Liu, J.; Li, X.-B.; Wang, D.; Lau, W.-M.; Peng, P.; Liu, L.-M. Diverse and tunable electronic structures of single-layer metal phosphorus trichalcogenides for photocatalytic water splitting. *J. Chem. Phys.* **2014**, *140*, 054707. [[CrossRef](#)]
28. Nathanson, M.; Kanhaiya, K.; Pryor, A.; Miao, J.; Heinz, H. Atomic-Scale Structure and Stress Release Mechanism in Core-Shell Nanoparticles. *ACS Nano* **2018**, *12*, 12296–12304. [[CrossRef](#)]